Structure of the full kinetoplastids mitoribosome and insight on its large subunit maturation

Heddy Soufari[1*] & Florent Waltz[1*], Camila Parrot[1+], Stéphanie Durrieu[1+], Anthony Bochler[1], Lauriane Kuhn[2], Marie Sissler[1], Yaser Hashem[1‡]

[1] Institut Européen de Chimie et Biologie, U1212 Inserm, UMR5320 CNRS, Université de Bordeaux, 2 rue R. Escarpit, F-33600 Pessac, France
[2] Plateforme protéomique Strasbourg Esplanade FRC1589 du CNRS, Université de Strasbourg, Strasbourg, France

*contributed equally, co-first authors
+contributed equally, co-second authors
‡corresponding author

Kinetoplastids are unicellular eukaryotic parasites responsible for human pathologies such as Chagas disease, sleeping sickness or Leishmaniasis (*1*)**. They possess a single large mitochondrion, essential for the parasite survival** (*2*)**. In kinetoplastids mitochondrion, most of the molecular machineries and gene expression processes have significantly diverged and specialized, with an extreme example being their mitochondrial ribosomes**(*3*)**. These large complexes are in charge of translating the few essential mRNAs encoded by mitochondrial genomes** (*4*, *5*)**. Structural studies performed in *Trypanosoma brucei* already highlighted the numerous peculiarities of these mitoribosomes and the maturation of their small subunit** (*3*, *6*)**. However, several important aspects mainly related to the large subunit remain elusive, such as the structure and maturation of its ribosomal RNA** (*3*)**. Here, we present a cryo-electron microscopy study of the protozoans *Leishmania tarentolae* and *Trypanosoma cruzi* mitoribosomes. For both species, we obtained the structure of their mature mitoribosomes, complete rRNA of the large subunit as well as previously unidentified ribosomal proteins. Most importantly, we introduce the structure of an LSU assembly intermediate in presence of 16 identified maturation factors. These maturation factors act both on the intersubunit and solvent sides of the LSU, where they refold and chemically modify the rRNA and prevent early translation before full maturation of the LSU.**

Kinetoplastids are unicellular eukaryotic parasites, causative agents of several human and livestocks pathologies (*1*). They are potentially lethal, affecting more than 20 million people worldwide (*1*). In part due to their parasitic nature, they strongly diverged from other eukaryotic model species. Kinetoplastids evolved to live in and infect a large variety of eukaryotic organisms in very different molecular environments. Consequently, beyond the general similarities, kinetoplastids species have diverged evolutionarily from each other and their protein sequence identity can be relatively low (*7*). They possess a single large mitochondrion, a crucial component of their cellular architecture, where gene expression machineries have also largely diverged, notably their mitochondrial ribosomes (mitoribosomes) (*3–5*, *8–10*). These sophisticated RNA-proteins complexes translate the few mRNAs still encoded by mitochondrial genomes. The mitoribosomes composition and structure greatly diverged from their bacterial ancestor, with the most extreme case described to date being in fact the kinetoplastids mitoribosomes. With highly reduced rRNAs, and more than 80 supernumerary ribosomal proteins (r-proteins) compared to bacteria, completely reshaping the overall ribosome structure. Recent structural studies performed in *Trypanosoma brucei* have highlighted the particularities of this mitoribosome structure and composition as well as the assembly processes of the small subunit (SSU) (*3*, *6*). However, in spite of the very comprehensive structural characterization of the full *T. brucei* SSU and its maturation, several pivotal aspects related to the LSU remained uncharacterized. For instance, a large portion of the LSU at the intersubunit side, including the whole rRNA peptidyl-transfer centre (PTC) along with several r-proteins where unresolved (*3*). Moreover, in contrast to the SSU, nearly nothing is known about the LSU maturation and assembly. More generally, the maturation of the mitoribosomes in all eukaryotic species remains largely underexplored. Here, we present a cryo-EM investigation of the full mature mitoribosomes from two different kinetoplastids, *Leishmania tarentolae* (*L. tarentolae*) and *Trypanosoma cruzi* (*T. cruzi*). Most importantly, we reveal

the structure of an assembly intermediate of the LSU displaying unprecedented details on rRNA maturation in these very singular mitoribosomes, some of which can probably be generalized for the maturation of all rRNA.

In order to obtain high-resolution reconstructions of the full kinetoplastids mitoribosomes, we purified mitochondrial vesicles from both *L. tarentolae* and *T. cruzi*, and directly purified the mitoribosomes from sucrose gradient (see Methods). All of our collected fractions were analyzed by nano-LC MS/MS (Table S1 and S2) in order to determine their proteomic composition. We collected micrographs from multiple vitrified samples corresponding to different sucrose-gradient density peaks for both species and following image processing we obtained cryo-EM reconstructions of the full mitoribosomes, but also the dissociated SSU. Most importantly, we also derived reconstructions of what appeared to be an assembly intermediate of *L. tarentolae* LSU. After extensive rounds of 2D and 3D classification and refinement we obtained the structure of *L. tarentolae* and *T. cruzi* complete and mature mitoribosomes at 3.9 Å and 6 Å, respectively (Fig. S1, S2 and S3). Other notable features include the intersubunit contacts and two distinct rotational states in *T. cruzi*. Similarly to *T. brucei* (*3*), our cryo-EM analysis revealed a reconstruction of an early initiation complex from *T. cruzi* at 3.1 and 3.2 Å for the body and the head of the SSU, respectively (Fig. S5). Further focused refinement on the LSU, SSU head and SSU body generated reconstructions at 3.6, 3.8 and 4 Å, respectively for *L. tarentolae* (Fig. S1 and S2), and 3.7 and 4.5 Å for *T. cruzi* LSU and SSU, respectively (Fig. S3). Combined, these reconstructions, along with the mass-spectrometry data allowed to build nearly complete atomic models, with only few protein densities still remaining unidentified.

General description of mature kinetoplastids mitoribosomes

Even though *T. cruzi* and *L. tarentolae* proteins are of relative modest sequence identity (~70%) for such closely related species (*7*), the tertiary structures of the r-proteins and rRNAs as well as the overall structure of the mitoribosomes were nearly entirely identical (Fig. S4). Both ribosomes are large complexes mainly formed by proteins (Fig. 1 and Fig. S5), 68 in the LSU and 54 in the SSU (Fig. S2 and Table S3), rRNA constituting only 15% of the total mass. The SSU was reconstructed to high resolution and appears similar to what was previously observed (*3*, *6*). We obtained reconstructions of the latter in the context of the full ribosomes from *L. tarentolae* and *T. cruzi*, but also dissociated in the context of what appears to be a partial initiation complex from *T. cruzi*, bound to mt-IF3, which accumulated naturally in our samples (Fig. 1 and Fig. S5). In the presence of mt-IF3, the 9S rRNA, in particular the highly reduced helix 44, and uS12m are clearly stabilized. However, in the context of the full ribosome, mt-IF3 is no longer present and the 9S rRNA along with uS12m at the subunit interface are significantly more flexible resulting in a scanter resolution. The reason of the accumulation of these SSU/mt-IF3 complexes is unclear but could reflect a relative low level of translation initiation in *T. cruzi*, at least at the growth stage at which the parasites were harvested. An additional explanation could be the fairly high hydrophobicity index of uS12m that is one of the only two r-proteins (along with uS3m) encoded by the mitochondrial genome in kinetoplastids. Indeed, recruiting such a hydrophobic r-protein to the negatively charged rRNA surface may require the presence of mt-IF3 that appears to stabilize it on the SSU intersubunit face rRNA (Fig. S5). In such case, these SSU/mt-IF3 complexes would correspond to an SSU ready to initiate translation. The biological rational for the presence in kinetoplastids mitoribosomes of such an rRNA-unfit protein at this strategic region remains to be unveiled but could already suggest a regulatory role for uS12m in the nuclear-mitochondrial crosstalk. Moreover, for the *T. cruzi* mitoribosome reconstruction, two distinct rotational states are observed, strongly suggesting a fully assembled mitoribosome structure capable of undergoing different conformational states (Fig. S3). In contrast to what is observed in prokaryotes and other mitoribosomes, very few of the intersubunit bridges are strictly conserved and most of them rely on protein-protein interactions. However, most of the observed intersubunit bridges are spatially conserved as compared to other known ribosomes but involve here kinetoplastid-specific r-proteins. (Fig. S6).

The reconstruction of the large subunit derived from the full mature ribosome (Fig. 1) allowed us to build the entire 12S rRNA including domains IV and V at the interface subunit (Fig. 1B-C), revealing the catalytic PTC, as well as its intertwined interactions with r-proteins. The structure of the domains V and IV is globally conserved, even when compared to classical prokaryotic ribosomes. Among the 68 LSU characterized proteins, uL2m, uL14m, and extensions of bL19m, mL68, previously unaccounted for (*3*), were visualised and detected by mass-spectrometry (Fig. 2). These proteins and extensions squeeze through the rRNA and stabilize it in a very intricate manner, compared to the classical prokaryotic and cytosolic ribosomes. Surprisingly, compared to what was previously described on the solvent side of the LSU, proteins mL67, mL71, mL77, mL78 and mL81, localized close to the peptide channel exit, are absent (Fig. 1 and 2) compared to the large subunit of *T. brucei*

(*3*). However, these proteins are present in the assembly intermediate, as described and discussed hereafter.

General description of the LSU assembly intermediate

During *L. tarentolae* 3D classification a class of particles presenting LSU-like features was found to naturally accumulate in our sample (Fig. S1). This class is rather distinct from classical LSU classes observed previously. After refinement and post-processing, this class resulted in a 3.4 Å reconstruction of the complex (Fig. 1). This reconstruction, when compared to the mature LSU, allowed us to visualize significant differences. Indeed, a large portion of the 12S rRNA appears to be unfolded, or at least highly flexible at the intersubunit face. In addition, large well resolved protein densities were observed occupying the position of the rRNA at this region. Moreover, the whole central protuberance (CP) was missing and several additional protein densities were observed on the solvent side (Fig.1E-F). Therefore, it clearly appeared that this complex corresponds to an LSU assembly intermediate. Our cryo-EM reconstructions, along with the MS/MS analysis, allowed us to build an atomic model of this LSU assembly intermediate (Fig. 2D-E). Compared to the mature LSU, this assembly intermediate lacks 18 core r-proteins and includes 16 maturation factors (including mL67, mL71, mL77, mL78 and mL81 that were previously described as r-proteins (*3*)). On the interface, domain IV of the 12S rRNA appears unfolded and several portions of the rRNA undergo refolding or modifications.

Solvent side

On the solvent side, close to the peptide channel exit, a crown of proteins composed of mL67, mL71, mL77, mL78 and mL81 was observed in the assembly intermediate (Fig. 3), but not on the full mature mitoribosome. The analysis of their structure and interaction network can suggest two main roles. Parts of them hold the 3' and 5' extremities of the 12S rRNA. Indeed, the 5' end of the 12S rRNA is surrounded by several positively charged residues of mL67 coordinating and stabilizing this extremity (Fig. 3A). On the 3' end, mL67 again, with the help of mL81 as well as r-proteins bL17m and mL85, stabilize this extremity that is more flexible in the mature LSU (Fig. 3B), as suggested by its scanter density. Hence, in the context of the assembly intermediate, these proteins, mainly mL67, hold both 12S rRNA extremities, most likely stabilizing the rRNA in its r-protein shell during its maturation.

Moreover, next to the rRNA extremities, the peptide channel exit is entirely remodeled compared to the mature LSU, as proteins mL71, mL77, mL78 reshape the peptide exit. These proteins slightly extend and split the channel exit in two parts (Fig. 3C). However, the channel itself is completely blocked by the N-terminal part of mL71, which therefore would prevent active translation (Fig. 3D), similarly to mL45 in mammalian mitoribosomes (*11*). Upon maturation, these factors are disengaged and a classical peptide channel is restored, similar in structure to bacterial ribosomes (Fig. 3C-D). Hence, we hypothesize that these proteins, previously observed in *T. brucei* (*3*), are actually maturation factors and that the LSU reconstruction of *T. brucei* is more likely to be a late assembly intermediate (Fig. 6B). Upon their dissociation from the mature LSU, a novel protein that we termed mL109 replaces mL67 and marks the maturation of this region (Fig. 3).

Intersubunit side

On the intersubunit side, a large portion of the 12S rRNA, corresponding to domain IV, appears unfolded and several proteins occupy its position, acting on the immature domain V. Based on high resolution cryo-EM reconstructions coupled with MS/MS analysis and structural and sequence homologies, 11 factors were identified bound to the intersubunit side. We termed these proteins "mt-LAFs" for mitochondrial LSU assembly factors, in accordance with the proposed nomenclature (*6*). Some of these factors belong to the family of GTPases and RNA helicases/isomerases, classic actors of ribosome biogenesis and were observed with their respective ligands and rRNA targets (Fig. 5E). Others are RNA modification enzymes. Part of these factors exhibit homology with bacterial and eukaryotic maturation factors previously identified. However, most of these ribosome maturation factors have never been structurally captured in an assembly intermediate context.

The first noticeable difference with the mature LSU is the absence of central protuberance (CP). Indeed, 8 proteins composing the CP are missing and some of the surrounding proteins observe different conformations (Fig. S7). In the assembly intermediate, the binding of the CP block is prevented by mt-LAF1 and mt-LAF6 (Fig. 4A and Fig. S7). The factor mt-LAF1 is a DEAD-box RNA helicase, where both the catalytic and ATP-binding sites are conserved, and the ATP ligand is clearly observed (Fig. 5E). It occupies the spatial positions of bL27m, bL31m, bL33m and mL82. The role of this family of helicase proteins is to unwind RNA structures and/or RNA-protein complexes, thus they are highly involved in ribosome maturation. Mt-LAF1 showed highest similarity with Has1, previously

described in yeast pre-60S maturation and with Mss116, involved in yeast mitoribosome maturation (*12*, *13*). Here, it contacts two different segments of the 12S rRNA, one single strand (residues 968-975) and the tip of H37 loop (residues 341-346). It thus appears to be involved in the maturation of helices H75 and H37 to allow their long-distance interaction in the mature subunit. The second factor, mt-LAF6, is in direct contact with mt-LAF1, but does not contact rRNA. Compared to the mature LSU, it occupies the place of mL38, mL69 and mL82. It shows high homology with tRNA pseudouridine synthases, however the active site is not conserved (Fig. S8A), hinting that the protein has lost its original function here. Its role seems to be a placeholder for CP r-proteins, and to act together with mt-LAF1 to prevent the CP r-proteins premature association. Hence, when mt-LAF 1 and 6 are disengaged, the CP r-proteins (composed of 8 proteins) can dock onto the LSU (Fig. S7). Moreover, the mL59/64 C-terminal part that is flexible in the assembly intermediate can contact and stabilize the CP in the mature LSU context.

Regarding the 12S rRNA, a large part is unfolded, which corresponds to the entire domain IV (Fig. S9), and several maturation factors are present in the region that will later be occupied by the rRNA after its maturation, including a triptych of GTPases, mt-LAF3, mt-LAF4 and mt-LAF5 (Fig. 4C). While some of these GTPase have already been identified in bacteria (Table S3), this is the first time that they are observed acting together on a maturating ribosomal complex at the reported resolution. GTPases have widespread roles in the cell (*14*). These enzymes usually exist in two states, active and inactive, where the transition between the states is triggered by GTP hydrolysis. This results in conformational changes of the enzyme that allows its binding to or release from specific targets. The mt-LAF5 has two characteristic G-domains, similarly to its bacterial homologue, EngA, also known as GTPase Der (*15*). Its role is crucial for domain IV PTC folding in bacteria, a role that is likely conserved here for mt-LAF5 given that their binding sites are similar. mt-LAF4 is bound to H54 and appears here to prevent uL2m association. Mt-LAF3 (homolog to the bacterial GTPase RgbA (*16*)) is in contact with mt-LAF 5 and 2. However, it is the only GTPase that does not make significant contacts with the rRNA (Fig. 4C), suggesting that it has either already performed its function, or is still awaiting for its rRNA target (Fig. S8B). The protein mt-LAF2 is a pseudouridine synthase D family enzyme that shows high homology with RluD, a conserved bacterial enzyme responsible for the modification of several residues on H69 in domain IV of 23S rRNA (*17*, *18*). In our reconstruction, we clearly observe a uridine residue flipped-out of the secondary structure to engage the catalytic core of the enzyme (Fig. 5D), strongly suggesting that this factor is catalytically functional.

Another distinctive feature of the immature rRNA is the structure of the P-stalk. Indeed, the P-stalk undergoes drastic structural rearrangements between an immature state, where it is shaped into two adjacent helices (Fig. 5A), and the mature P-stalk (Fig. 5C). Interestingly, even though the fold is radically different, the immature P-stalk rRNA still spans all the way and interacts with uL11m (Fig. 5B). While the nearby homodimeric factors mt-LAF7.a/mt-LAF7.b are in close proximity to the rRNA, they cannot be unambiguously interpreted to bind it directly. mt-LAF7.a/mt-LAF7.b contact uL11m and mL53 inducing the shift of the P-stalk r-protein block compared to the mature structure. Moreover, several surrounding r-proteins such as uL10m or uL16m are absent. Mt-LAF7 a and b being RNA 2'O-methyltransferases, it is possible that they have either already modified or will modify the P-stalk rRNA. The latter will thus be reshaped into its mature structure afterwards, probably under the action of a helicase analogue to LAF1 (Fig. S8C).

Lastly, a complex formed by three assembly factors is found bound to uL14m, close to the P-stalk. This complex is formed by mt-LAF8, directly contacting uL14m and the tip of H95 (residues 1133-1136), mt-SAF32 and mt-LAF9 (Fig. 4B). This complex is nearly identical to the MALSU1:L0R8F8:mt-ACP complex observed in the human mitoribosome LSU assembly intermediate (*19*). Indeed, each factor shows high homology to their mammalian homologs, mt-LAF9 corresponding to L0R8F8, mt-SAF32 to mt-ACP and finally mt-LAF8 to MALSU1. The latter shows high homology to the conserved and well characterized bacterial ribosome silencing factor (RsfS) (Fig. S8D). RsfS is known to prevent premature subunit association during diminished nutrient availability, a molecular mechanism mimicked by eIF6 in eukaryotes (*20*, *21*). However, in mitoribosomes, as shown in human, the RsfS homolog alone is not able to prevent subunit association and the anti-subunit association activity can only be achieved in the presence of mt-SAF32 and mt-LAF9. The natural accumulation of the LSU assembly intermediate in our sample could be promoted by the presence of the mt-LAF8:mt-SAF32:mt-LAF9 complex, which might be stress-induced or caused by diminished nutrient availability, likewise in bacteria. Interestingly, as its name already indicates, SAF-32 is also found in the SSU assembly intermediates, likewise at a peripheral position of the intersubunit side (*6*). Finally, SAF-32 and mt-LAF9 are both respiratory complex I components (*22*, *23*) suggesting a dual role of these

proteins and hinting at a possible crosstalk between mitoribosome maturation and respiratory complex assembly.

Conclusions

In conclusion, our cryo-EM structures of kinetoplastids mitoribosomes, especially the yet unobserved LSU assembly intermediate, shed new lights into ribosome maturation. Even though several proteins are specific to kinetoplastids, most of the maturation factors present in our structure have homologs in other eukaryotes, mitochondria or bacteria (Table S3). Hence, our structure unveils the mode of actions of these factors, for which no high-resolution structures in native conditions exist. It also highlights that even though highly divergent, kinetoplastids mitoribosomes retained several canonical maturation pathways for their rRNAs. We hypothesize that, even in a highly divergent system, some maturation steps are conserved and follow an analogous mechanistic pattern (Fig. 6). Indeed, in concert, a set of factors intercalate with the premature rRNA (GTPases) to mechanically unpack different premature rRNA domains, allowing RNA helicases to disentangle and unwind the rRNA and several families of modification enzymes to access their targets. The remodeling of the rRNA is also aided by the recruitment of the r-proteins early during the maturation process. This is especially true in the kinetoplastids mitochondria, where most of the r-proteins are already recruited at the observed stage and form a thick protein shell holding the rRNA together. At the same time, various anti-association factors prevent premature binding of r-proteins and the SSU joining.

In spite of large environmental and host diversities in which these parasites evolve, their mitoribosomes are conserved structurally among kinetoplastids. Therefore, our structures could serve as a basis for future experiments to develop more effective and safer kinetoplastid-specific therapeutic strategies. Finally, as kinetoplastids undergo extensive mitochondrial reorganization (*24*) during their life cycle, both in vectors and hosts, it would also be interesting to study mitoribosomes from different stages of development from the parasite's life cycle.

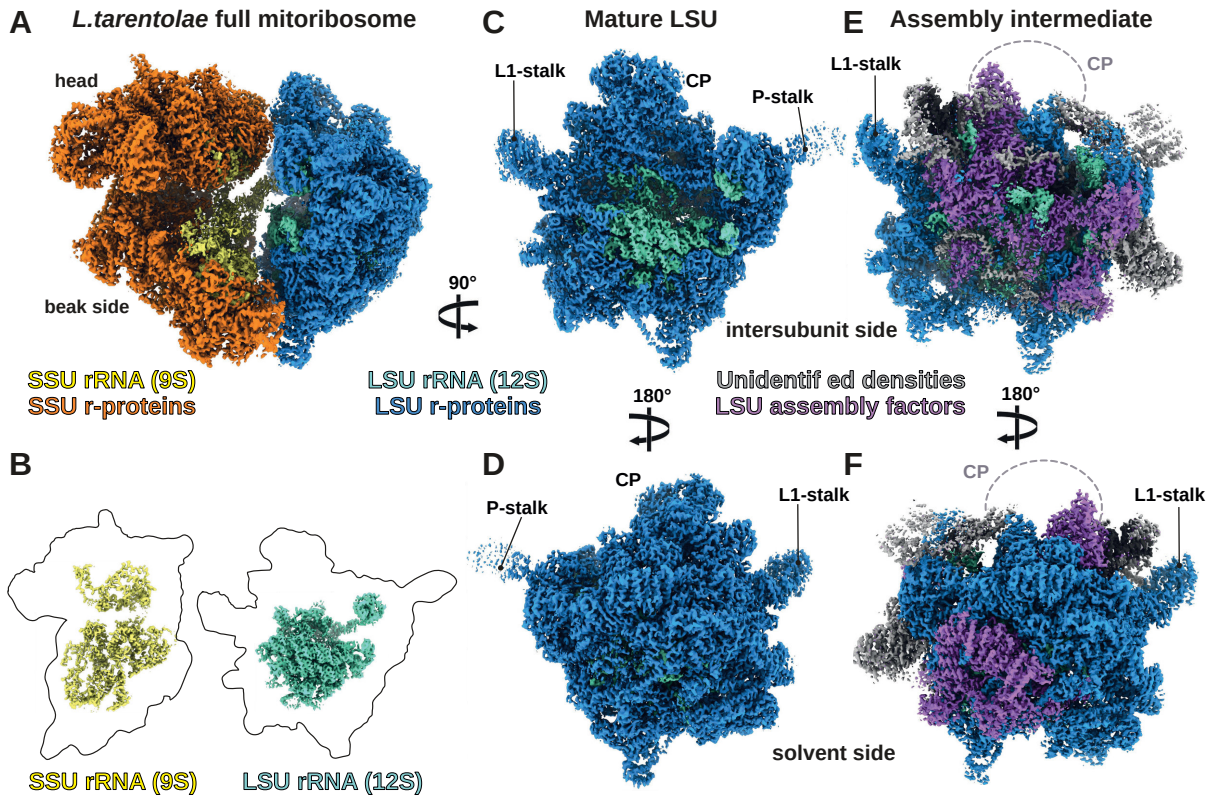

Figure 1. Cryo-EM reconstructions of the mature and assembly intermediate *L. tarentolae* mitoribosome (**A**) Composite cryo-EM map of the full and mature mitoribosome of *L. tarentolae.* SSU is depicted in orange shades, with proteins in orange and rRNA in yellow and LSU is depicted in blue, with proteins in dark blue and rRNA in aquamarine. (**B**) Relative sizes of the rRNA (colored segmented densities) compared to that of the r-proteins (presented as thick black contours). (**C** and **D**) present the cryo-EM reconstructions of the mature LSU viewed from the intersubunit (**C**) and solvent (**D**) side, compared with the LSU assembly intermediate subunit (**E-F**). Densities corresponding to assembly factors are shown in purple, grey correspond to unidentif ed factors.

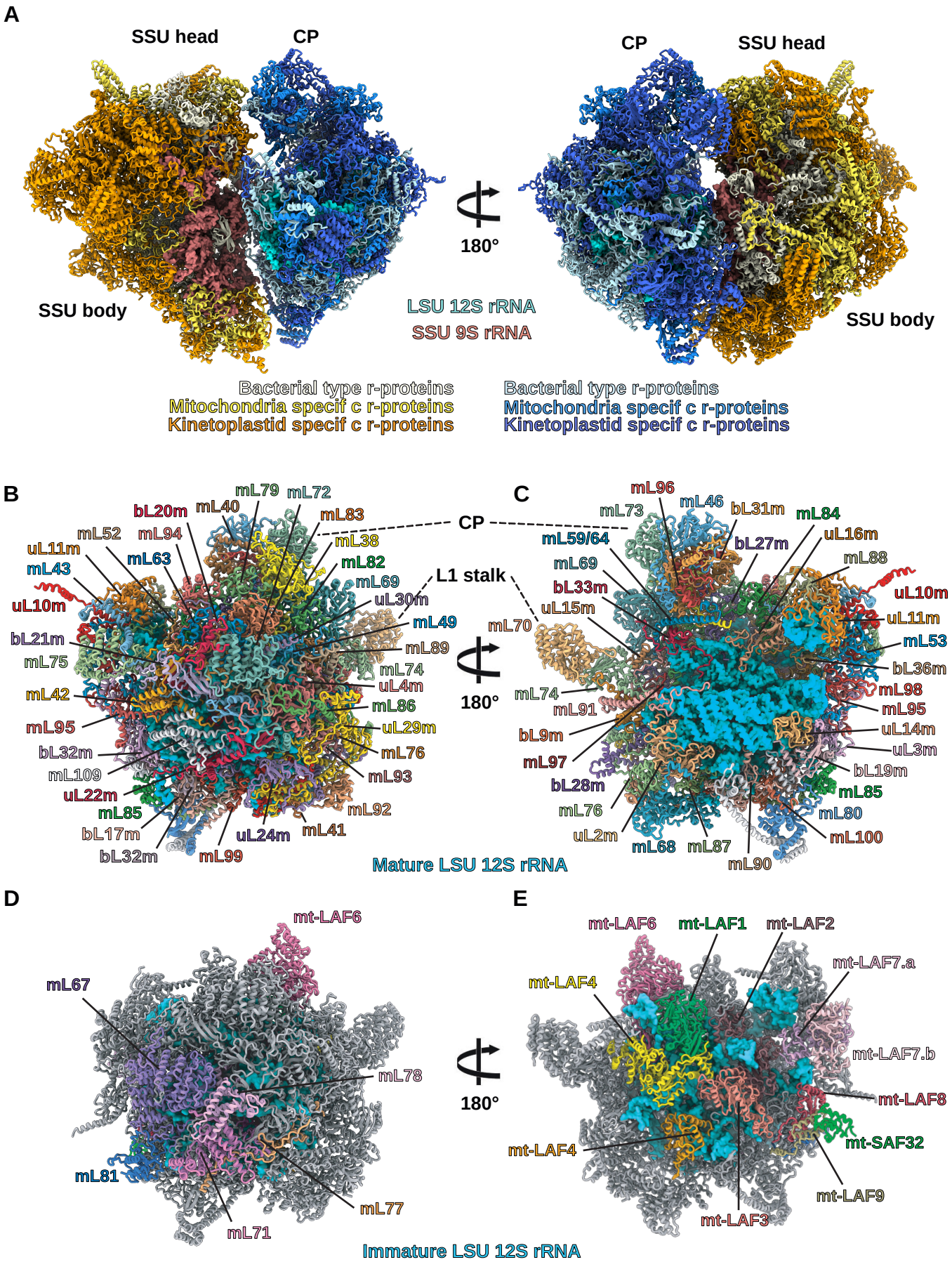

Figure 2. Atomic models of *L. tarentolae* mitoribosome and LSU assembly intermediate

(**A**) Overall model of *L. tarentolae* mitoribosome. 12S rRNA is colored in cyan (LSU) and the 9S rRNA in brick (SSU). Ribosomal proteins are colored in shades of blue (LSU) and shades of yellow (SSU), according to their conservation. Solvent side (**B**) and intersubunit side (**C**) of the mature LSU with each individual r-proteins annotated and displayed with a dif erent color. Solvent side (**D**) and intersubunit side (**E**) of the LSU assembly intermediate. Conserved proteins in the mature LSU (**B-C**) are depicted in gray and assembly factors are colored in dif erent shades and individually annotated.

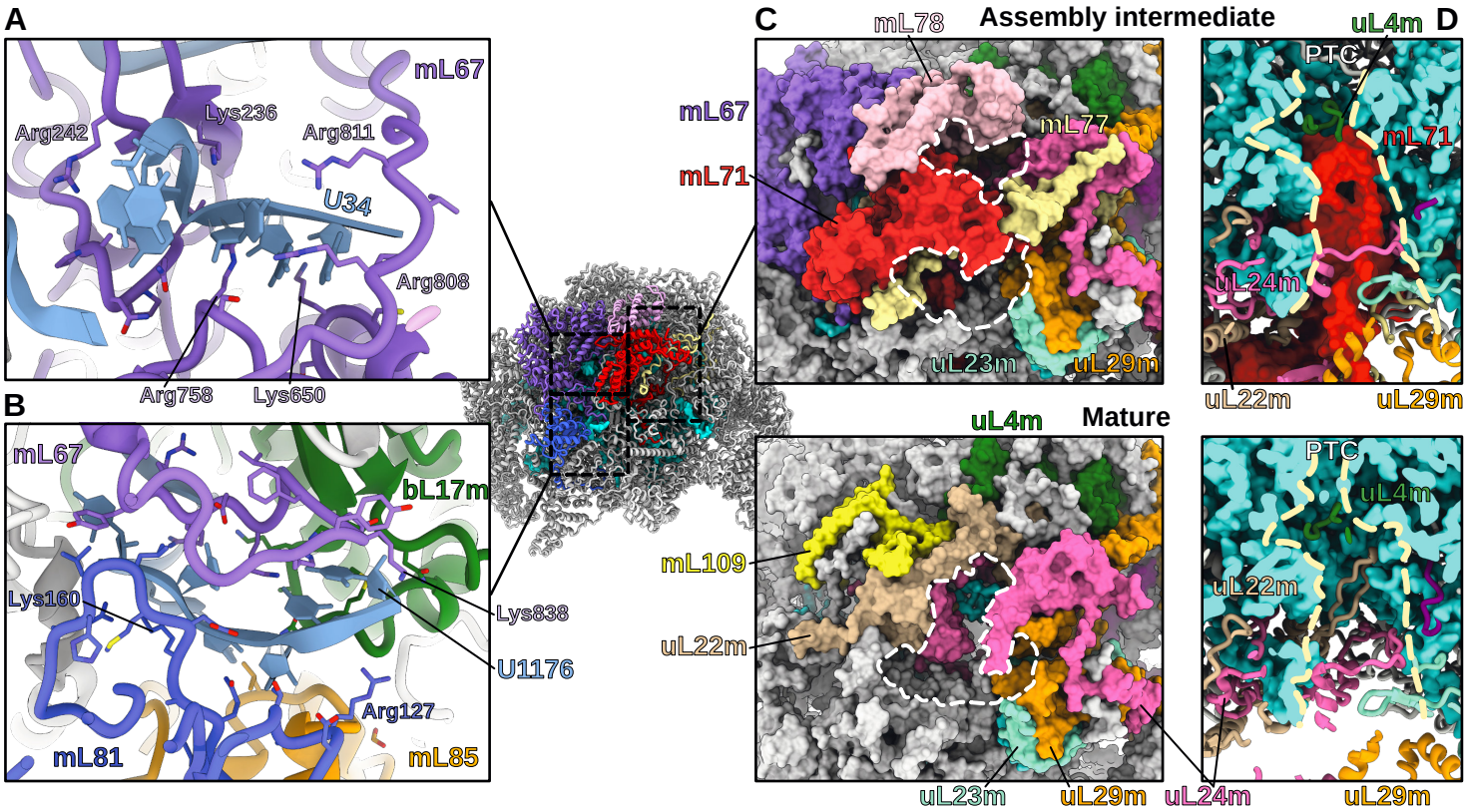

Figure 3. Specif c factors hold the 12S rRNA termini and probe the peptide channel exit on the solvent side of the immature LSU

On the solvent side, 5 maturation factors act together to hold the extremities of the rRNA (**A-B**) and probe the peptide exit channel (**C-D**). The 12S 5' termini (**A**) is held by several positively charged residues of mL67, and the 3' extremity (**B**) is stabilized by mL67 and mL81 as well as r-proteins mL85 and bL17m. U34 and U1176 indicate the terminal rRNA residues. (**C** and **D**) present the peptide channel of the assembly intermediate (top) and mature (bottom) LSU from top (**C**) and cut view (**D**). Proteins mL71, mL77, mL78 reshape the peptide exit channel by slightly extending and splitting it in two in the assembly intermediate compared to the mature LSU (**C**). Dashed white contours delimit the peptide channel exit orif ces in the mature and immature LSU. Maturation factor mL71 completely blocks the exit channel through its N-terminal domain (**D**). Dashed yellow lines delimit the peptide channel in the longitudinal axis.

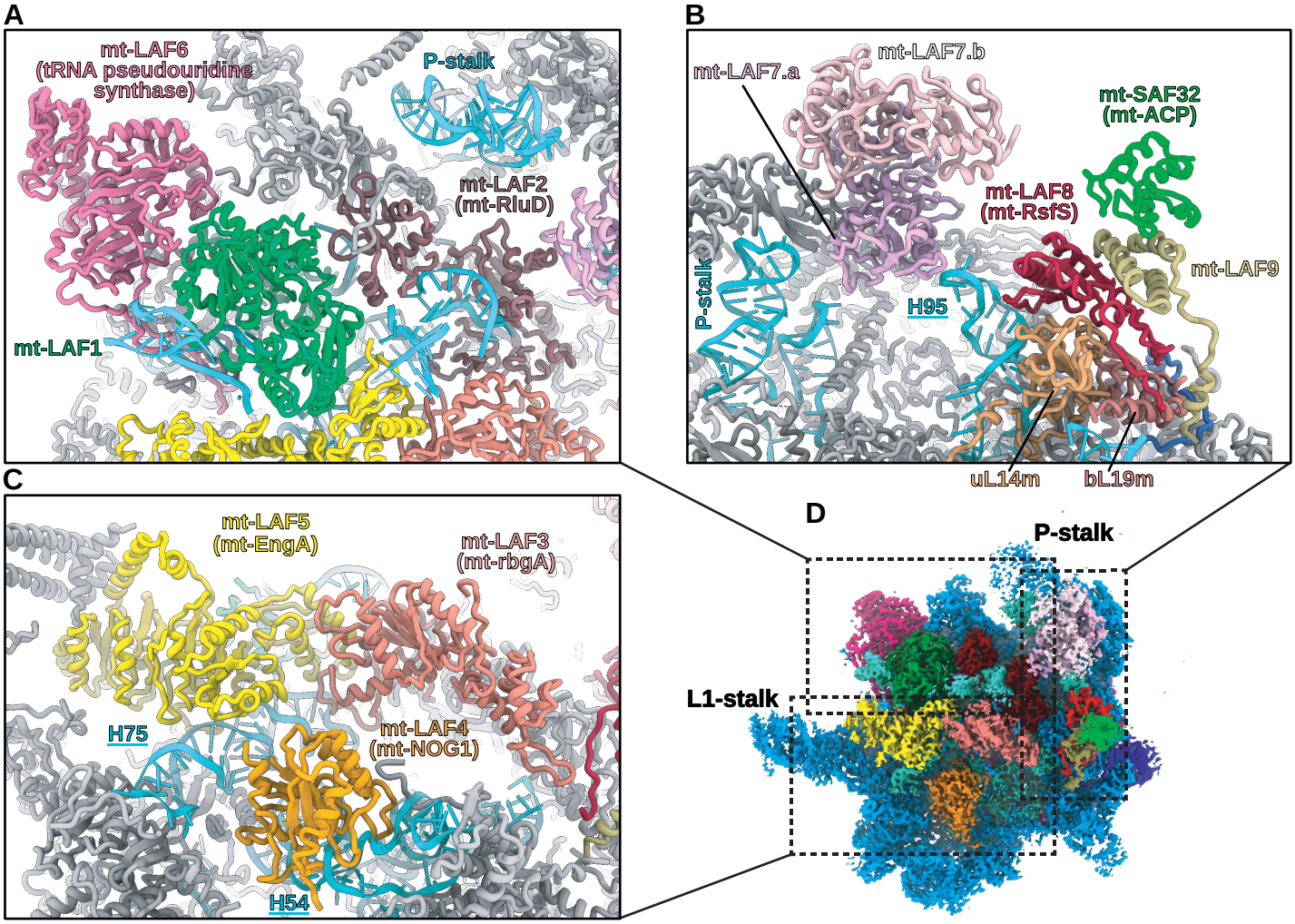

Figure 4. Overall view of the maturation factors on the intersubunit side

On the intersubunit side of the immature LSU, 11 maturation factors act together to remodel and modify the rRNA (**D**). (**A**) mt-LAF6 and mt-LAF1 occupy the position of the central protuberance (CP). mt-LAF1 and mt-LAF2 interact with remodeled rRNA. (**B**) Mt-LAF8 together with mt-LAF9 and mt-SAF32 interact with uL14m and H95 to block the SSU association. (**C**) Arrangement of the GTPase triptych. The GTPases mt-LAF5 and mt-LAF4 bind respectively the rRNA H75 and H37 while mt-LAF3 occupies a central place in the complex and makes a bridge between the GTPases and mt-LAF2 and mt-LAF8.

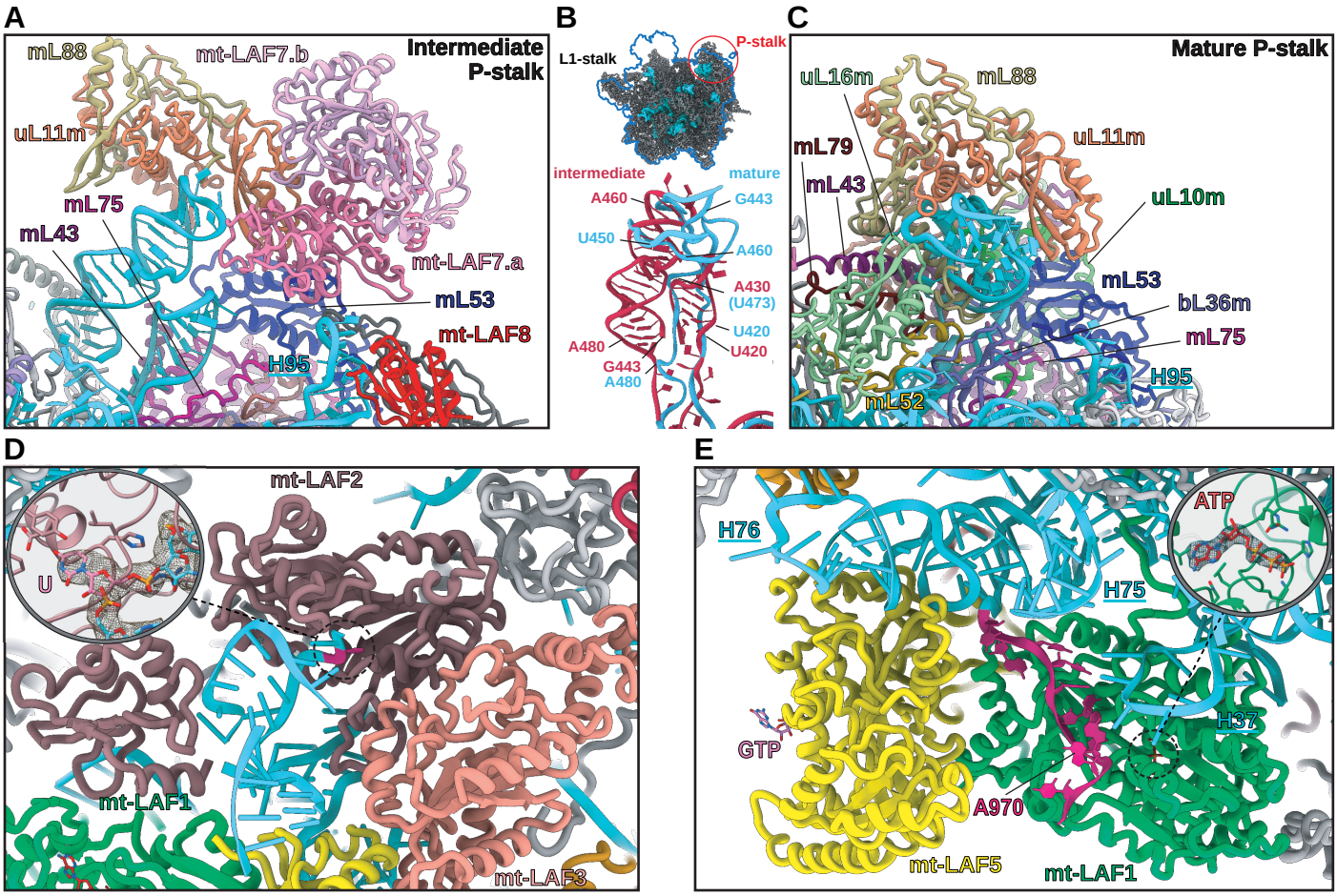

Figure 5. Maturation of the Leishmania mitochondrial LSU rRNA

Details on how maturation factors interact with, and af ect the 12S RNA (**A**) P-stalk region of the intermediate LSU. mt-LAF7 homodimer contacts uL11m and mL53, the two helices of the immature P-stalk as well as the helix H95 are adjacent to the dimer. (**B**) Overlap of the two forms of rRNA P-stalk structure, immature in red and mature in blue. (**C**) P-stalk region of the mature LSU. (**D**) Insight into the rRNA modif cation by the pseudouridine synthase mt-LAF2. In order to be catalyzed the rRNA is refolded into a helix structure, probably to be recognized by mt-LAF2, the uridine subtract is f ipped out of the helix and engaged in the catalytic core of the enzyme. (**E**) The two factors mt-LAF5 and mt-LAF1 bind jointly to the rRNA. The dead box helicase mt-LAF1 is in an active state with a single strand RNA in its catalytic core and loaded with an ATP molecule. Doted circle corresponds to magnif ed region.

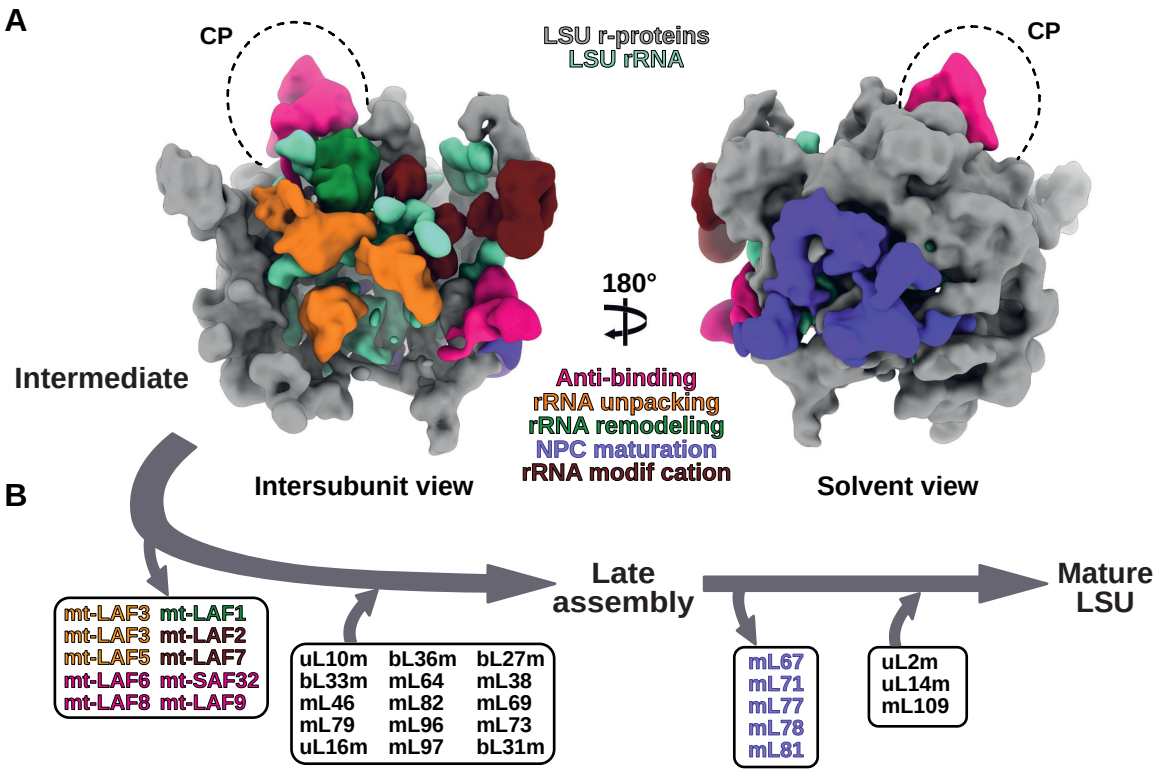

Figure 6. Schematic view and roles of the dif erent assembly factors

(**A**) Schematic view of the LSU assembly intermediate of *L. tarentolae* presented from the intersubunit and solvent sides. Maturation factors are colored by function. Starting from the LSU assembly intermediate in (**A**)**,** (**B**) details the dissociation of maturation factors and the association of r-proteins, considering the *T. brucei* LSU (*3*) as a late assembly intermediate. Maturation factors are colored as in (**A**) and r-proteins are shown in black.

METHODS

Methods and any associated references are available in the online version of the paper.

ACKNOWLEDGEMENTS

This work has benefitted from the facilities and expertise of the Biophysical and Structural Chemistry platform (BPCS) at IECB, CNRS UMS3033, Inserm US001, Bordeaux University. We thank A. Bezault for assistance with the Talos Arctica electron microscope. We thank J. Chicher and P. Hamman of the Strasbourg Esplanade proteomic analysis for the proteomic analysis.

Funding

This work was funded by a European Research Council Starting Grant (TransTryp ID:759120) and the IdEx junior excellence chair program of the Université de Bordeaux to YH and the French National Program “Investissement d’Avenir” (Labex MitoCross), administered by the "Agence National de la Recherche", and referenced [ANR-11-LABX-0057_MITOCROSS] to MS. This project was supported by "Institut National de la Santé et de la Recherche Médicale" (INSERM), "Centre National de la Recherche Scientifique" (CNRS) and Université de Bordeaux.

Author contributions

YH, HS and FW designed and coordinated the experiments. CP and SD purified kinetoplastids mitochondria. FW purified mitoribosomal complexes. LK performed the mass-spectrometry experiments. HS acquired the cryo-EM data and processed the cryo-EM results with YH and FW. HS, YH, FW and AB built the atomic models. FW, HS, MS and YH interpreted the structures. FW, HS, CP, YH and MS wrote and edited the manuscript. YH directed the research.

Competing interests

The authors declare no competing financial interests.

Data and materials availability

The cryo-EM maps of the mitoribosome have been deposited at the Electron Microscopy Data Bank (EMDB) with accession codes XXXX. Corresponding atomic models have been deposited in the Protein Data Bank (PDB) with PDB codes XXXX. The mass spectrometry proteomics data have been deposited to the ProteomeXchange Consortium via the PRIDE partner repository with the dataset identifier PXDxxxxx.

ONLINE METHODS

Purification of *T. cruzi* and *L. tarentolae* mitochondria

For mitochondria purification, protocols adapted from Hauser et al. 1996 (*26*) and Schneider et al. 2007 (*27*) were used. Quickly, cells were re-suspended in SoTE buffer (600 mM sorbitol, 20 mM Tris-HCl pH 7.5, 1 mM EDTA) to a final concentration of 2.5×10^9 cells/ml and lysed by nitrogen cavitation at 80 bar for 1 hour. After pressure release the lysate was centrifuged and resuspended in SoTM buffer (600 mM sorbitol, 20 mM Tris-HCl pH 7.5, 5 mM $MgCl_2$) for DNase I treatment during 15 minutes. EDTA was added to stop DNAse treatment and the sample was centrifuged, resuspended in 2 volumes of SoTE containing 50% Histodenz™ (Sigma Aldrich D2158). For *L. tarentolae* the fraction was loaded onto a 21.7%/25%/28.3/31.6% Histodenz™ step gradients. Gradients were centrifuged for 45 minutes at 100,000 g and the mitochondrial fraction was collected at the 25%/28.3% interface. For *T. brucei* the fraction was loaded onto a 18%/21%/25%/28% Histodenz™ step gradient and the mitochondrial fraction was collected at the 21%/25% interface.

Purification of mitochondrial ribosomes

For mitoribosome purification, protocols adapted from Waltz & Soufari et al. (*10*) were applied. Quickly, mitochondria were re-suspended in Lysis buffer (20 mM HEPES-KOH, pH 7.6, 100 mM KCl, 20 mM $MgCl_2$, 1 mM DTT, 1 % Triton X-100, 2 % DDM, supplemented with proteases inhibitors (Complete EDTA-free) to a concentration of 1 mg/mL and incubated for 15 min in 4°C. Lysate was clarified by centrifugation at 30.000 g, 20 min at 4°C. The supernatant was loaded on a 40% sucrose cushion in Monosome buffer (same as lysis buffer without Triton X-100 and with 0.02% DDM) and centrifuged at 235.000 g, 3h, 4°C. The crude ribosomes pellet was re-suspended in Monosome buffer and loaded on a 10-30% sucrose gradient in the same buffer and run for 16 h at 65,000 g. Fractions corresponding to mitoribosomes were collected, pelleted and re-suspended in Monosome buffer.

Grid preparation

4 µL of the samples at a concentration of 2 µg/µl was applied onto Quantifoil R2/2 300-mesh holey carbon grid, which had been coated with thin home-made continuous carbon film and glow-discharged. The sample was incubated on the grid for 30 sec and then blotted with filter paper for 2 sec in a temperature and humidity controlled Vitrobot Mark IV (T = 4°C, humidity 100%, blot force 5) followed by vitrification in liquid ethane pre-cooled by liquid nitrogen.

Single particle cryo-electron microscopy data collection

For the two data-sets (Full and dissociated complexes), data collection was performed on a Talos Arctica instrument (Thermofisher) at 200 kV using the EPU software (Thermofisher) for automated data acquisition. Data were collected at a nominal underfocus of -0.5 to -2.7 µm at a magnification of 120,000 X yielding a pixel size of 1.24 Å. Micrographs were recorded as movie stack on a Falcon III direct electron detector (Thermofisher), each movie stack were fractionated into 20 frames for a total exposure of 1 sec corresponding to an electron dose of 60 ē/Å2.

Electron microscopy image processing

Drift and gain correction and dose weighting were performed using MotionCor2 (*28*). A dose weighted average image of the whole stack was used to determine the contrast transfer function with the software Gctf (*29*). The following process has been achieved using RELION 3.0 (*30*). Particles were picked using a Laplacian of gaussian function (min diameter 280 Å, max diameter 480 Å). *L. tarentolae* full mitoribosome, after 2D classification, 303,140 particles were extracted with a box size of 400 pixels and binned four fold for 3D classification into six classes. Three classes depicting high-resolution features, consisting of 82,060 particles, were selected for refinement, yielding 3.9 Å resolution. After focused refinement with a mask on the LSU, the body and the head of the SSU, 3.6, 4 and 3.8 Å resolution were respectively obtained. For the assembly intermediate of the LSU, after 2D classification, 215,120 particles were extracted with a box size of 400 pixels and binned three fold for 3D classification into 8 classes. Two classes, consisting of 59,200 particles, depicting high-resolution features were selected for refinement, yielding 3.4 Å resolution.

For the *T. cruzi* full mitoribosomes reconstruction, 126,340 particles were selected after 3D classification for refinement, resulting in a 6 Å resolution reconstruction, which was further refine to 3.7 Å and 4.5 Å resolution for the LSU and SSU respectively. For the *T. cruzi* mt-IF3 SSU complex, 148,180 particles were selected after 3D classification for refinement, resulting in a 3.5 Å resolution reconstruction, which was further refine to 3.1 Å and 3.2 Å resolution for the SSU body and SSU head respectively. Determination of the local resolution of the final density map was performed using ResMap (*25*).

Structure building and model refinement

The atomic models of the kinetoplastid mitoribosomes were built into the high-resolution maps using Coot, Phoenix and Chimera. Atomic models from *E. coli* ribosome (5kcr) (*31*), and trypanosoma mitoribosome (6hiv) (*3*) were used as starting points for protein identification and modelisation. For the Leishmania mitoribosome, atomic models were build using *L. major* protein sequences due to the poor quality of *L. tarentolae* available data. The online SWISS-MODEL service was used to generate initial models for bacterial and mitochondria conserved r-proteins. Models were then rigid body fitted to the density in Chimera (*32*) and all subsequent modeling was done in Coot (*33*). For the LSU ribosomal RNA, the 23S rRNA from *E.coli* was docked into the maps and used as template from positioning and reconstruction. Punctual differences were done in Chimera using the “swapna” command line and the model was then further refined in Coot. The global atomic model was refined with VMD using the Molecular Dynamic Flexible Fitting (MDFF) then with PHENIX using a combination of real and reciprocal space refinement for proteins.

Proteomic and statistical analyses of mitochondrial ribosome composition

Mass spectrometry analyses of the ribosome fractions were performed at the Strasbourg-Esplanade proteomic platform and performed as previously (*10*, *34*). In brief, proteins were trypsin digested and mass spectrometry analyses were carried out by nano LC-ESI-MS/MS analysis on a Thermo QExactive+ mass spectrometer. Quantitative label-free proteomics analysis was performed through in-house bioinformatics pipelines.

Figure preparation

Figures featuring cryo-EM densities as well as atomic models were visualized with UCSF ChimeraX (*35*) and Chimera (*32*).

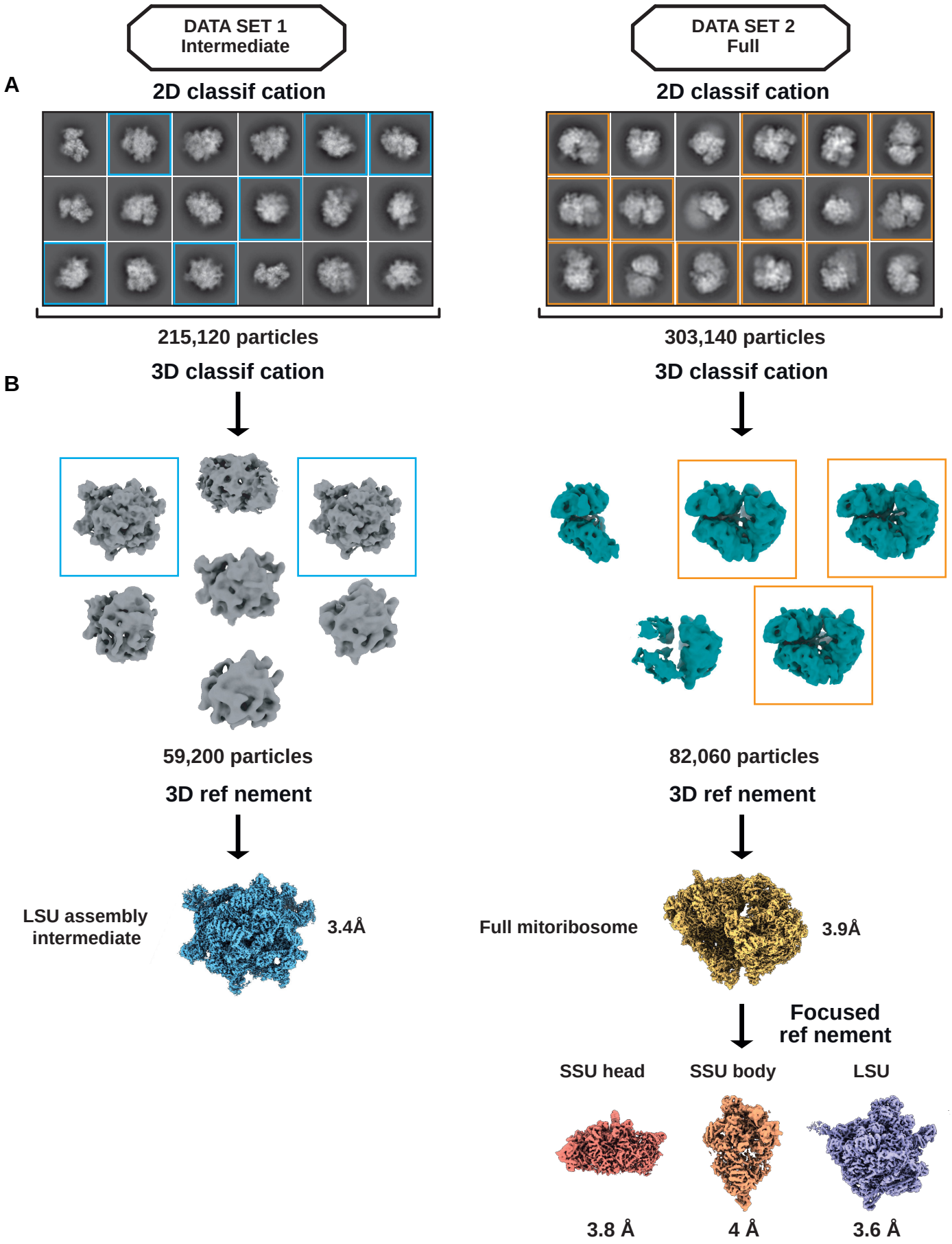

Supplementary Figure 1. Data processing workf ow of *L. tarentolae* data sets
Graphical summary of the processing workf ow described in Methods for the *L. tarentolae* samples, resulting in the LSU assembly intermediate for Data set 1 and the full mitoribosome for Data set 2. 2D classes are presented in (**A**) and 3D processing and ref nement presented in (**B**).

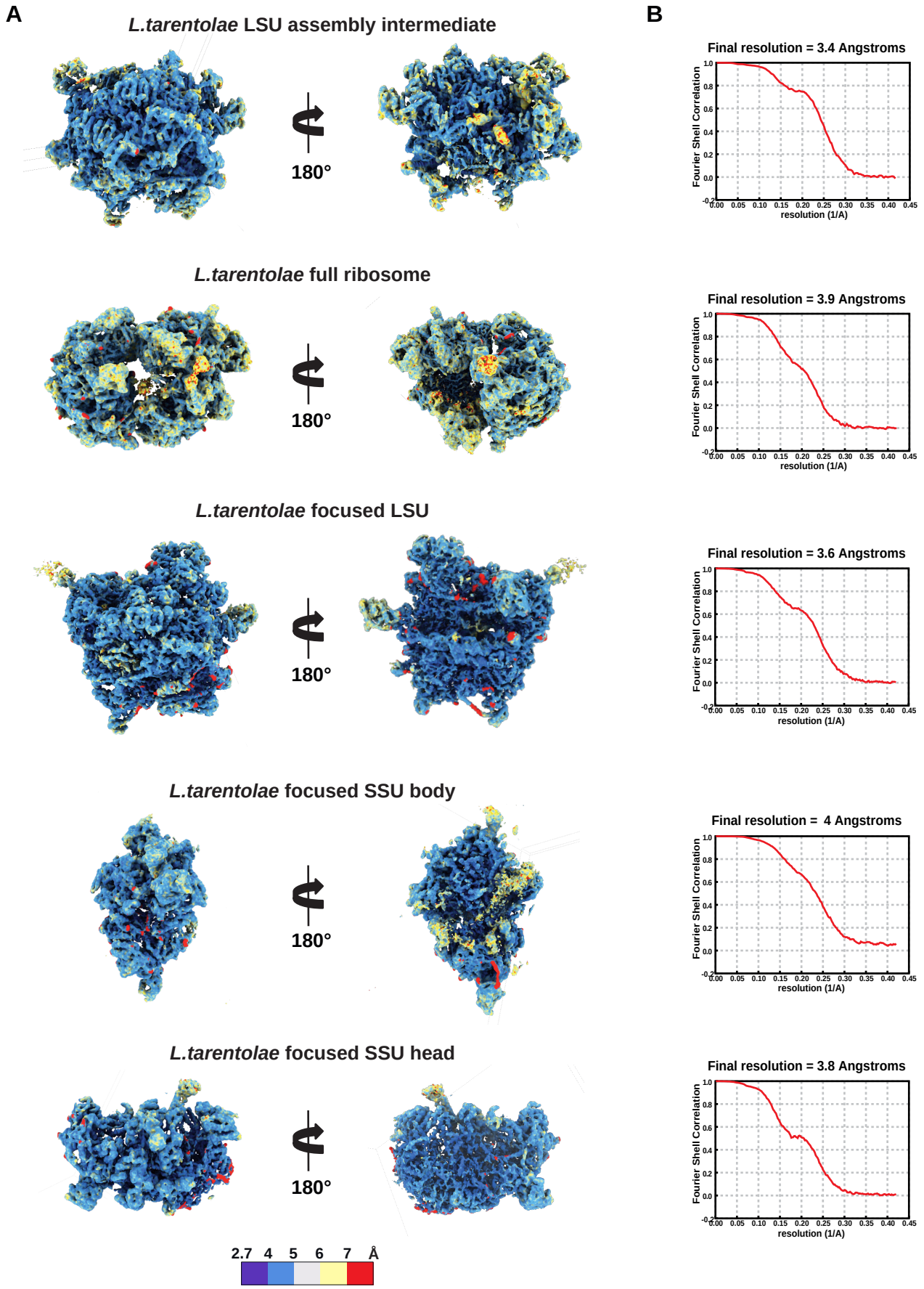

Supplementary Figure 2. Local resolution of *L. tarentolae* f nal reconstructions
Local resolutions of the dif erent reconstructions are presented. The maps are colored by resolution, generated using ResMap (*25*) (**A**). For both reconstructions FSC plots are displayed for resolution estimation (**B**). The map resolution is calculated at the 0.143 threshold.

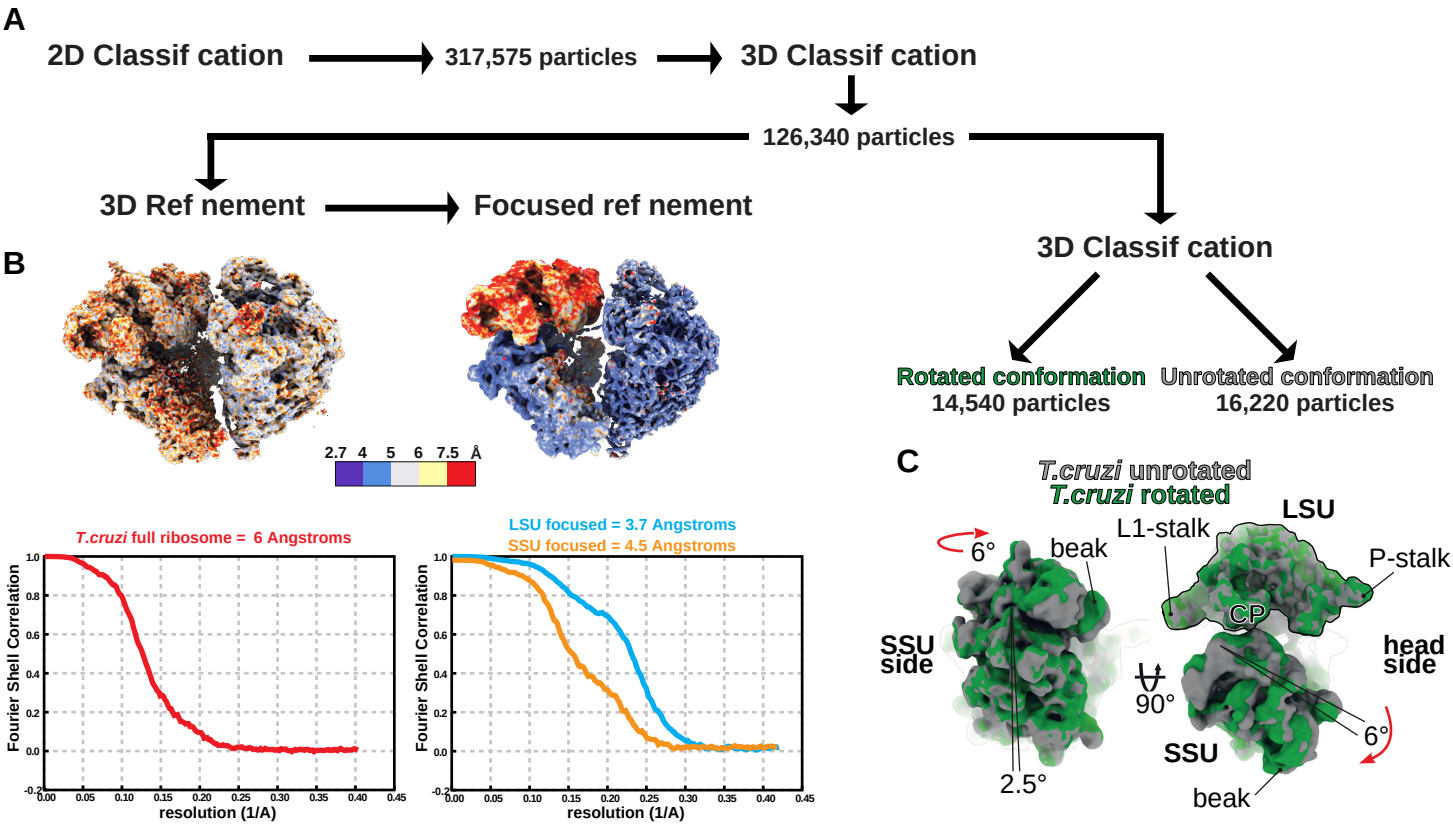

Supplementary Figure 3. Data processing of *T. cruzi* full mitoribosome

Graphical summary of the processing workf ow *T. cruzi* full mitoribosome. 2D classif cation and 3D processing are presented in (**A**) with respective ResMap (*25*) representation and FSC plots presented in (**B**). Second round of 3D classif cation lead to the identif cation of two rotational states presented in (**C**).

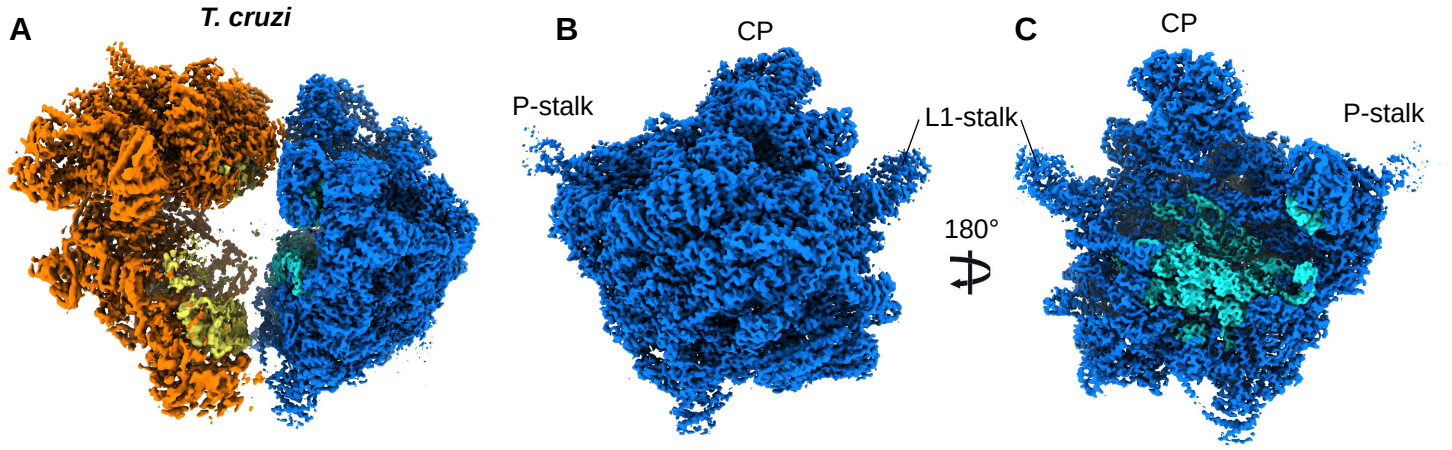

<u>Supplementary Figure 4. Cryo-EM reconstructions of *T. cruzi* mitoribosomes</u>
Cryo-EM reconstructions of *T. cruzi* full mitoribosome (**A**) as well as the mature LSU, seen from the solvent view (**B**) and the interface view (**C**). Compared with the *L.tarentolae* reconstructions presented in Figure 1, the ribosomes are nearly identical.

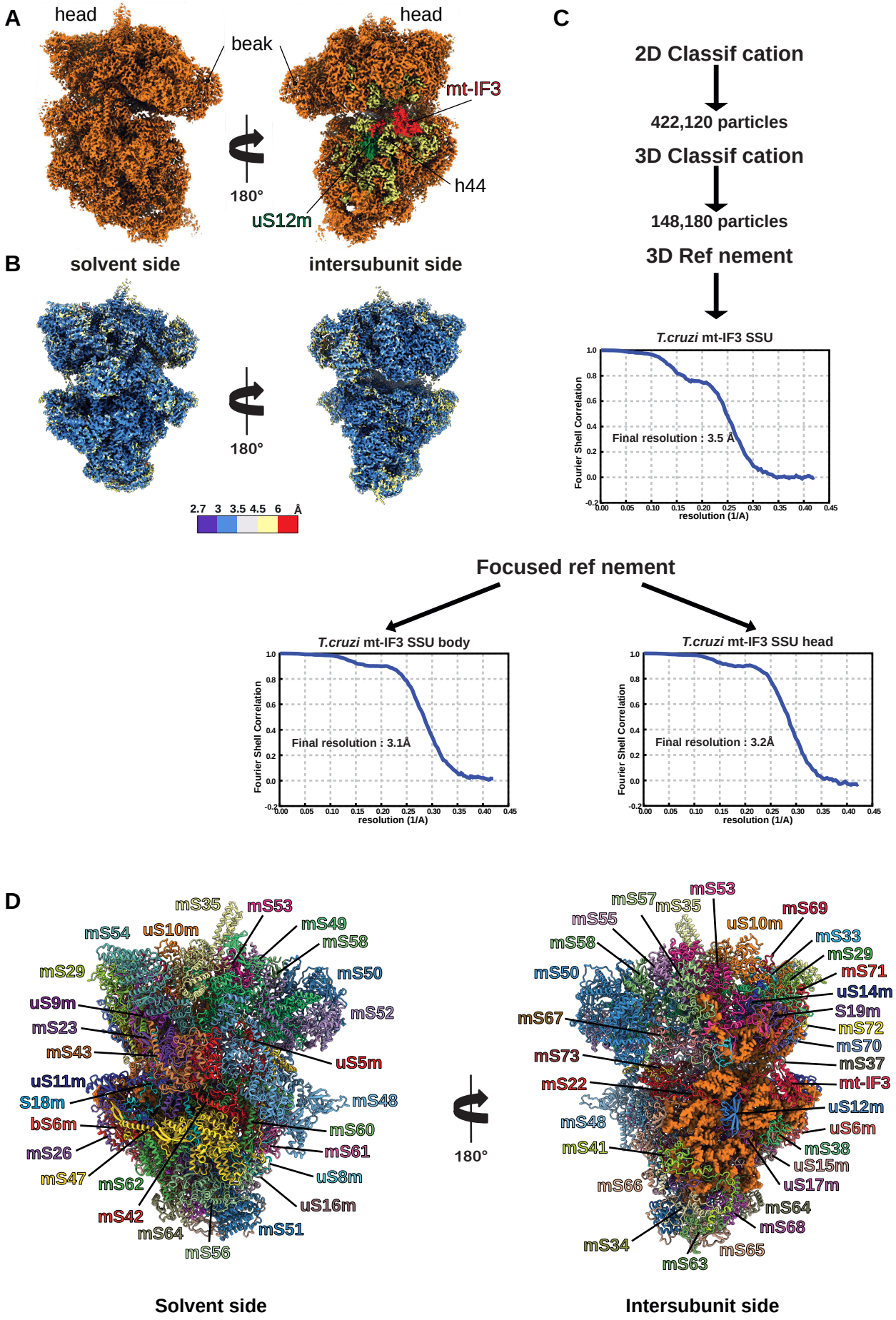

Supplementary Figure 5. Data processing and model of the mt-IF3 SSU of *T. cruzi*

Cryo-EM map reconstruction of the *T. cruzi* in presence of mt-IF3 is shown in (**A**), with r-proteins colored in orange, 9S rRNA in yellow, mt-IF3 in red and uS12m in green. Local resolution generated using ResMap (*25*) are shown in (**B**), and the processing workf ow with the respective FSC plots for initial and focused 3D ref nement are displayed in (**C**). The resulting atomic model is presented in (**D**), each r-proteins are individually annotated, 9S rRNA is colored in orange.

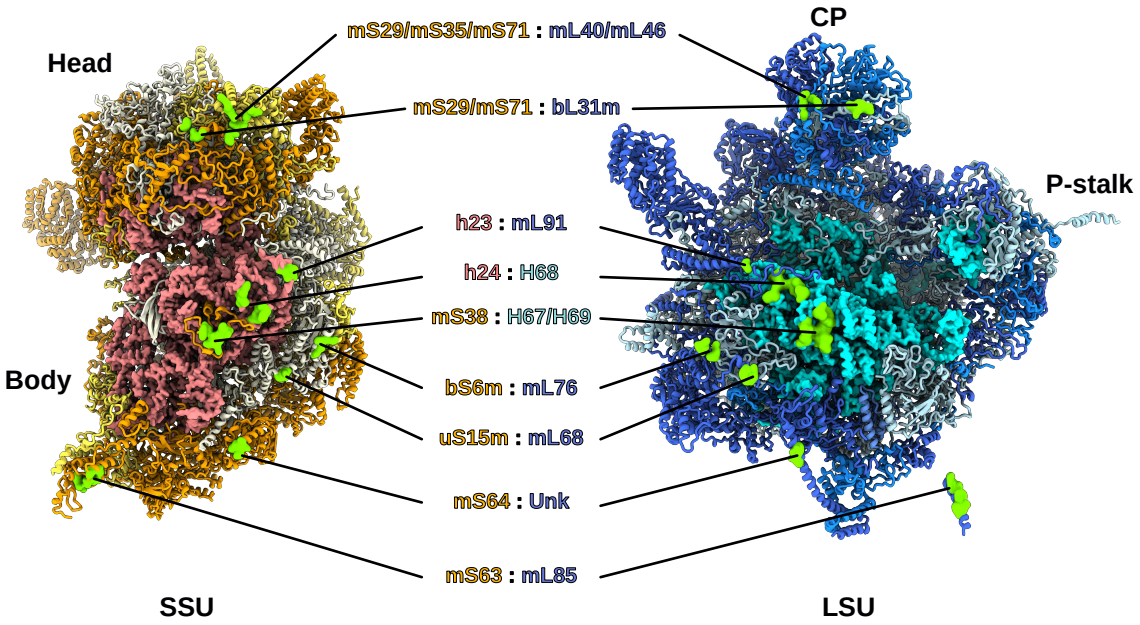

Supplementary Figure 6. Intersubunit bridges

List of the intersubunit bridges observed in the mature and full kinetoplastid mitoribosomes. Both the SSU and LSU are presented on the intersubunit side and bridge positions are indicated in green. Most of the bridges involve protein:protein interactions , except for the highly conserved rRNA:rRNA bridge between h24 and H68. Overall, the other bridge positions seem to be common with other mitoribosomes and bacterial ribosomes but involve mitochondria and kinetoplastid-specif c r-proteins, for example, bL31m is the only bacterial-type r-protein involved in the bridges between the SSU's head and LSU's CP. One truly kinetoplastid-specif c bridge is observed with mS63 and mL85, which involves kinetoplastid only r-proteins.

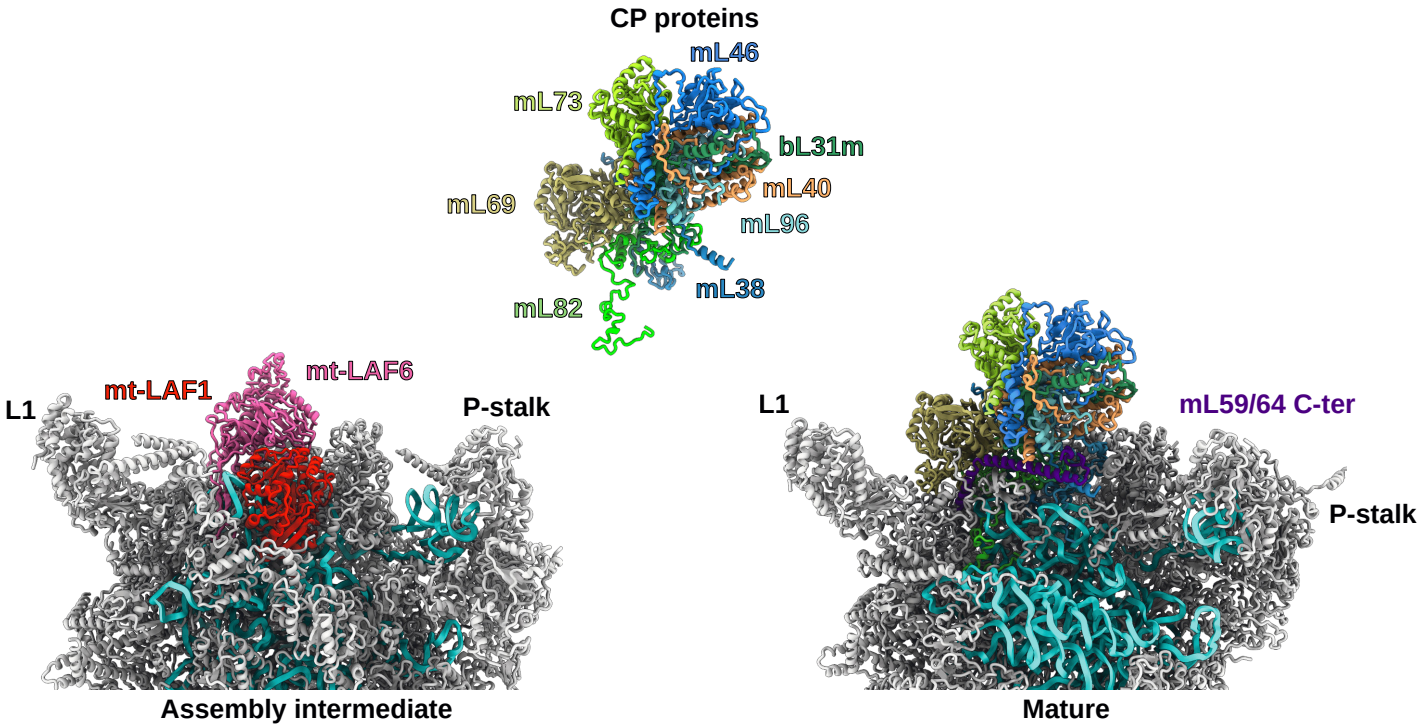

Supplementary Figure 7. Central protuberance maturation in Leishmania LSU
Comparison of the assembly intermediate and mature CP area of the LSU. In the assembly intermediate, CP proteins are prevented from binding by mt-LAF1 and mt-LAF6. Upon release of the maturation factors the whole CP block can dock the LSU and additional r-proteins contacting the CP, like bL33m and the C-terminus of mL59/64 can lock the structure. 12S rRNA is displayed in cyan.

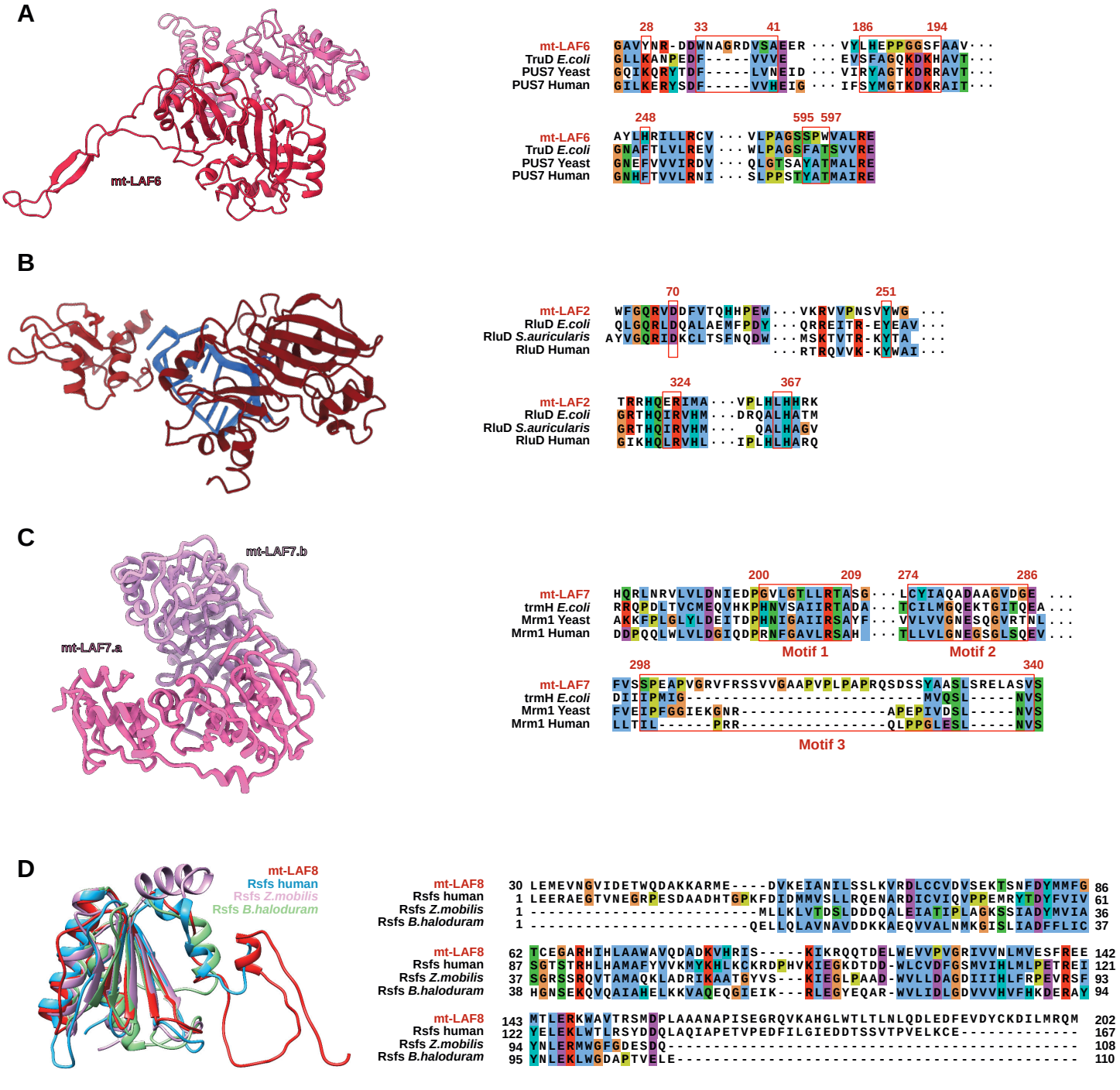

Supplementary Figure 8. Maturation factors compared with their homologues

Sequence alignments and structural comparison of the different maturation factors identified. In (**A**, **B** and **C**), conserved, or non-conserved, catalytic sites are highlighted by red boxes. (**A**) show that none of the catalytic sites of mt-LAF6 are conserved, mt-LAF6 is thus inactive. In (**B** and **C**) the conserved catalytic regions of mt-LAF2 and mt-LAF7 highlight that even though activity is not observed in our model (lack of ligand or target) these enzyme are still active. They most probably have already fulfilled their function or are waiting to perform it. In (**D**), complete alignment and structure superimposition of mt-LAF8 with bacterial Rsfs and the human mitochondrial one is shown. This shows high conservation of this protein but also highlight the presence a C-terminal extension, most likely involved in the interaction with the mitochondria specific mt-LAF9 (L0R8F8 in human) and mt-SAF32 (mt-ACP in human).

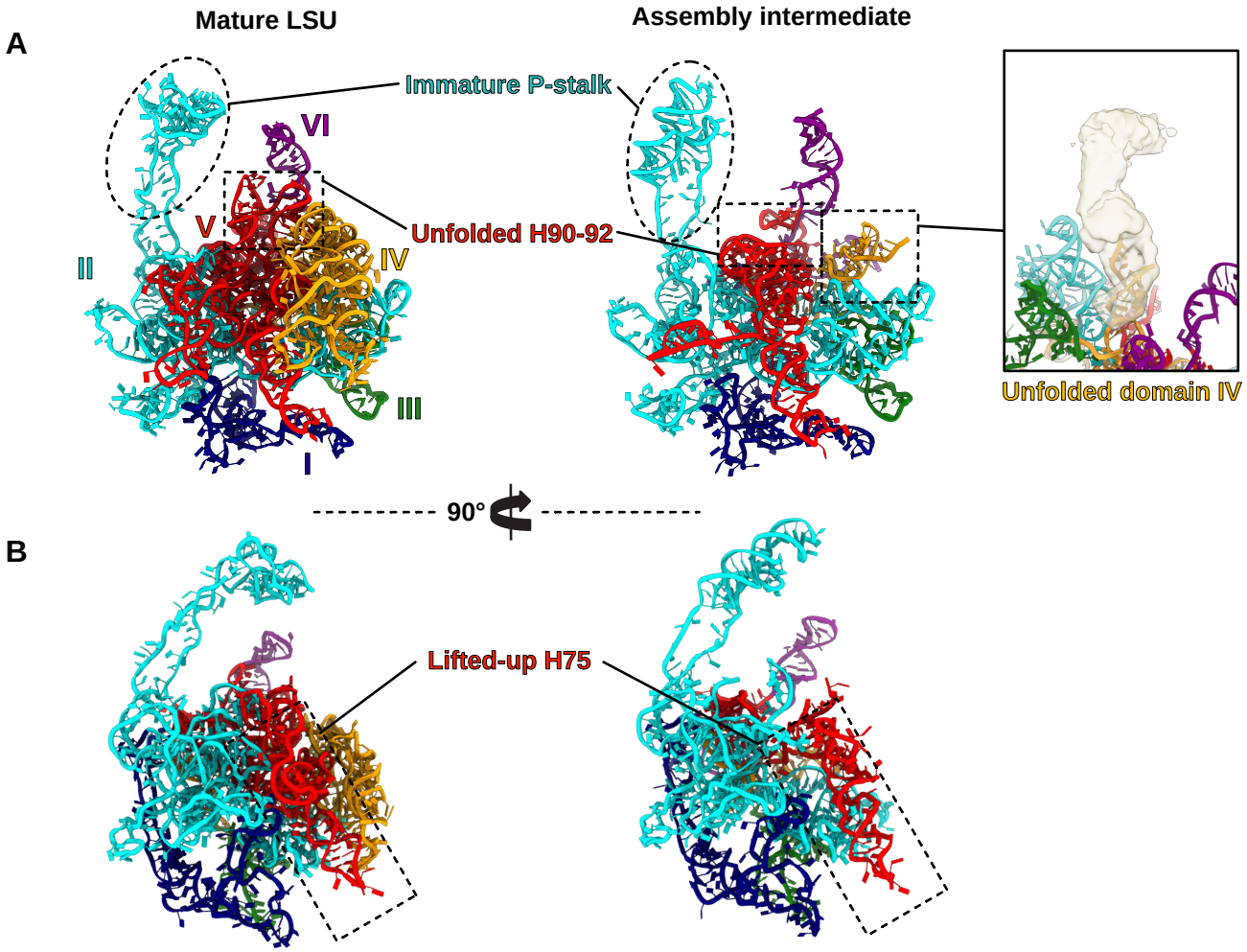

Supplementary Figure 9. 12 rRNA maturation

Comparison between mature and assembly intermediate 12S rRNA. Each domain are colored dif erently. The rRNA is presented from the intersubunit view (**A**) and a side view (**B**). The main dif erences are observed in domain II where the P-stalk is folded dif erently, in domain IV which is entirely unfolded, and domain V which is unfolded from H90 to H92 and where H75 is entirely lifted-up. Most of the maturation factors act on domain V which is accessible thanks to the unfolded domain IV.

References and notes

1. K. Stuart, R. Brun, S. Croft, A. Fairlamb, R. E. Gürtler, J. McKerrow, S. Reed, R. Tarleton, Kinetoplastids: related protozoan pathogens, different diseases. *J. Clin. Invest.* **118**, 1301–1310 (2008).
2. L. Simpson, O. H. Thiemann, N. J. Savill, J. D. Alfonzo, D. A. Maslov, Evolution of RNA editing in trypanosome mitochondria. *Proc. Natl. Acad. Sci.* **97**, 6986–6993 (2000).
3. D. J. F. Ramrath, M. Niemann, M. Leibundgut, P. Bieri, C. Prange, E. K. Horn, A. Leitner, D. Boehringer, A. Schneider, N. Ban, Evolutionary shift toward protein-based architecture in trypanosomal mitochondrial ribosomes. *Science.* **362**, eaau7735 (2018).
4. F. Waltz, P. Giegé, Striking Diversity of Mitochondria-Specific Translation Processes across Eukaryotes. *Trends Biochem. Sci.* **45**, 149–162 (2019).
5. P. Bieri, B. J. Greber, N. Ban, High-resolution structures of mitochondrial ribosomes and their functional implications. *Curr. Opin. Struct. Biol.* **49**, 44–53 (2018).
6. M. Saurer, D. J. F. Ramrath, M. Niemann, S. Calderaro, C. Prange, S. Mattei, A. Scaiola, A. Leitner, P. Bieri, E. K. Horn, M. Leibundgut, D. Boehringer, A. Schneider, N. Ban, Mitoribosomal small subunit biogenesis in trypanosomes involves an extensive assembly machinery. *Science.* **365**, 1144–1149 (2019).
7. A. P. Jackson, T. D. Otto, M. Aslett, S. D. Armstrong, F. Bringaud, A. Schlacht, C. Hartley, M. Sanders, J. M. Wastling, J. B. Dacks, A. Acosta-Serrano, M. C. Field, M. L. Ginger, M. Berriman, Kinetoplastid Phylogenomics Reveals the Evolutionary Innovations Associated with the Origins of Parasitism. *Curr. Biol.* **26**, 161–172 (2016).
8. N. Desai, A. Brown, A. Amunts, V. Ramakrishnan, The structure of the yeast mitochondrial ribosome. *Science.* **355**, 528–531 (2017).
9. A. Amunts, A. Brown, J. Toots, S. H. W. Scheres, V. Ramakrishnan, The structure of the human mitochondrial ribosome. *Science.* **348**, 95–98 (2015).
10. F. Waltz, H. Soufari, A. Bochler, P. Giegé, Y. Hashem, Cryo-EM structure of the RNA-rich plant mitochondrial ribosome. *Nat. Plants*. **6**, 377–383 (2020).
11. E. Kummer, M. Leibundgut, O. Rackham, R. G. Lee, D. Boehringer, A. Filipovska, N. Ban, Unique features of mammalian mitochondrial translation initiation revealed by cryo-EM. *Nature*. **560**, 263–267 (2018).
12. R. Zeng, E. Smith, A. Barrientos, Yeast Mitoribosome Large Subunit Assembly Proceeds by Hierarchical Incorporation of Protein Clusters and Modules on the Inner Membrane. *Cell Metab.* **27**, 645-656.e7 (2018).
13. D. Zhou, X. Zhu, S. Zheng, D. Tan, M.-Q. Dong, K. Ye, Cryo-EM structure of an early precursor of large ribosomal subunit reveals a half-assembled intermediate. *Protein Cell*. **10**, 120–130 (2019).
14. A. Wittinghofer, I. R. Vetter, Structure-Function Relationships of the G Domain, a Canonical Switch Motif. *Annu. Rev. Biochem.* **80**, 943–971 (2011).
15. X. Zhang, K. Yan, Y. Zhang, N. Li, C. Ma, Z. Li, Y. Zhang, B. Feng, J. Liu, Y. Sun, Y. Xu, J. Lei, N. Gao, Structural insights into the function of a unique tandem GTPase EngA in bacterial ribosome assembly. *Nucleic Acids Res.* **42**, 13430–13439 (2014).
16. P. Pausch, W. Steinchen, M. Wieland, T. Klaus, S.-A. Freibert, F. Altegoer, D. N. Wilson, G. Bange, Structural basis for (p)ppGpp-mediated inhibition of the GTPase RbgA. *J. Biol. Chem.* **293**, 19699–19709 (2018).
17. J. Sivaraman, P. Iannuzzi, M. Cygler, A. Matte, Crystal Structure of the RluD Pseudouridine Synthase Catalytic Module, an Enzyme that Modifies 23S rRNA and is Essential for Normal Cell Growth of Escherichia coli. *J. Mol. Biol.* **335**, 87–101 (2004).
18. P. P. Vaidyanathan, M. P. Deutscher, A. Malhotra, RluD, a highly conserved pseudouridine synthase, modifies 50S subunits more specifically and efficiently than free 23S rRNA. *RNA*. **13**, 1868–1876 (2007).
19. A. Brown, S. Rathore, D. Kimanius, S. Aibara, X. Bai, J. Rorbach, A. Amunts, V. Ramakrishnan, Structures of the human mitochondrial ribosome in native states of assembly. *Nat. Struct. Mol. Biol.* **24**, 866–869 (2017).
20. X. Li, Q. Sun, C. Jiang, K. Yang, L.-W. Hung, J. Zhang, J. C. Sacchettini, Structure of Ribosomal Silencing Factor Bound to Mycobacterium tuberculosis Ribosome. *Structure*. **23**, 1858–1865 (2015).
21. I. Khusainov, B. Fatkhullin, S. Pellegrino, A. Bikmullin, W. Liu, A. Gabdulkhakov, A. Al Shebel, A. Golubev, D. Zeyer, N. Trachtmann, G. A. Sprenger, S. Validov, K. Usachev, G. Yusupova, M. Yusupov, Mechanism of ribosome shutdown by RsfS in Staphylococcus aureus revealed by

integrative structural biology approach. *Nat. Commun.* **11**, 1656 (2020).
22. K. Parey, O. Haapanen, V. Sharma, H. Köfeler, T. Züllig, S. Prinz, K. Siegmund, I. Wittig, D. J. Mills, J. Vonck, W. Kühlbrandt, V. Zickermann, High-resolution cryo-EM structures of respiratory complex I: Mechanism, assembly, and disease. *Sci. Adv.* **5**, eaax9484 (2019).
23. A.-N. A. Agip, J. N. Blaza, H. R. Bridges, C. Viscomi, S. Rawson, S. P. Muench, J. Hirst, Cryo-EM structures of complex I from mouse heart mitochondria in two biochemically defined states. *Nat. Struct. Mol. Biol.* **25**, 548–556 (2018).
24. M. Jakob, A. Hoffmann, S. Amodeo, C. Peitsch, B. Zuber, T. Ochsenreiter, Mitochondrial growth during the cell cycle of Trypanosoma brucei bloodstream forms. *Sci. Rep.* **6**, 36565 (2016).
25. A. Kucukelbir, F. J. Sigworth, H. D. Tagare, Quantifying the local resolution of cryo-EM density maps. *Nat. Methods*. **11**, 63–65 (2014).
26. R. Hauser, M. Pypaert, T. Häusler, E. K. Horn, A. Schneider, In vitro import of proteins into mitochondria of Trypanosoma brucei and Leishmania tarentolae. *J. Cell Sci.* **109**, 517–523 (1996).
27. A. Schneider, N. Bouzaidi-Tiali, A.-L. Chanez, L. Bulliard, in *Methods in molecular biology (Clifton, N.J.)* (2007; http://www.ncbi.nlm.nih.gov/pubmed/18314740), vol. 372, pp. 379–387.
28. S. Q. Zheng, E. Palovcak, J.-P. Armache, K. A. Verba, Y. Cheng, D. A. Agard, MotionCor2: anisotropic correction of beam-induced motion for improved cryo-electron microscopy. *Nat. Methods*. **14**, 331–332 (2017).
29. K. Zhang, Gctf: Real-time CTF determination and correction. *J. Struct. Biol.* **193**, 1–12 (2016).
30. J. Zivanov, T. Nakane, B. O. Forsberg, D. Kimanius, W. J. Hagen, E. Lindahl, S. H. Scheres, New tools for automated high-resolution cryo-EM structure determination in RELION-3. *Elife*. **7** (2018), doi:10.7554/eLife.42166.
31. S. Arenz, M. F. Juette, M. Graf, F. Nguyen, P. Huter, Y. S. Polikanov, S. C. Blanchard, D. N. Wilson, Structures of the orthosomycin antibiotics avilamycin and evernimicin in complex with the bacterial 70S ribosome. *Proc. Natl. Acad. Sci.* **113**, 7527–7532 (2016).
32. E. F. Pettersen, T. D. Goddard, C. C. Huang, G. S. Couch, D. M. Greenblatt, E. C. Meng, T. E. Ferrin, UCSF Chimera--a visualization system for exploratory research and analysis. *J. Comput. Chem.* **25**, 1605–12 (2004).
33. P. Emsley, B. Lohkamp, W. G. Scott, K. Cowtan, Features and development of Coot. *Acta Crystallogr. Sect. D Biol. Crystallogr.* **66**, 486–501 (2010).
34. F. Waltz, T. Nguyen, M. Arrivé, A. Bochler, J. Chicher, P. Hammann, L. Kuhn, M. Quadrado, H. Mireau, Y. Hashem, P. Giegé, Small is big in Arabidopsis mitochondrial ribosome. *Nat. Plants*. **5**, 106–117 (2019).
35. T. D. Goddard, C. C. Huang, E. C. Meng, E. F. Pettersen, G. S. Couch, J. H. Morris, T. E. Ferrin, UCSF ChimeraX: Meeting modern challenges in visualization and analysis. *Protein Sci.* **27**, 14–25 (2018).